



Co-Processed Crystalline Solids of Ivermectin with Span® 60 as Solubility Enhancers of Ivermectin in Natural Oils

Luandri de Vos¹ · Minja Gerber¹ · Wilna Liebenberg¹ · Johanna C. Wessels¹ · Hendrik J. R. Lemmer¹

Received: 5 November 2023 / Accepted: 6 March 2024
© The Author(s) 2024

Abstract

Despite being discovered over five decades ago, little is still known about ivermectin. Ivermectin has several physico-chemical properties that can result in it having poor bioavailability. In this study, polymorphic and co-crystal screening was used to see if such solid-state modifications can improve the oil solubility of ivermectin. Span® 60, a lipophilic non-ionic surfactant, was chosen as co-former. The rationale behind attempting to improve oil solubility was to use ivermectin in future topical and transdermal preparations to treat a range of skin conditions like scabies and head lice. Physical mixtures were also prepared in the same molar ratios as the co-crystal candidates, to serve as controls. Solid-state characterization was performed using X-ray powder diffraction (XRPD), Fourier-transform infrared spectroscopy (FTIR), differential scanning calorimetry (DSC) and thermogravimetric analysis (TGA). The FTIR spectra of the co-crystal candidates showed the presence of Span® 60's alkyl chain peaks, which were absent in the spectra of the physical mixtures. Due to the absence of single-crystal X-ray data, co-crystal formation could not be confirmed, and therefore these co-crystal candidates were referred to as co-processed crystalline solids. Following characterization, the solid-state forms, physical mixtures and ivermectin raw material were dissolved in natural penetration enhancers, i.e., avocado oil (AVO) and evening primrose oil (EPO). The co-processed solids showed increased oil solubility by up to 169% compared to ivermectin raw material. The results suggest that co-processing of ivermectin with Span® 60 can be used to increase its oil solubility and can be useful in the development of oil-based drug formulations.

Keywords avocado oil · co-processing · evening primrose oil · natural penetration enhancer · physical mixtures · solid-state · Span® 60

Introduction

Avermectin was discovered by chance when microbiologist, Satoshi Ōmura, collected a soil sample in the woods close to a golf course located in Kawana, on the southeast coast of Honshu in Japan [1, 2]. Since the discovery of avermectins in the 1970s, a new class of compounds, namely endectocides (named after its potent activity against endoparasites and ectoparasites), was crafted [1, 3, 4]. Avermectins are produced naturally by the fermentation of *Streptomyces avermitilis*, an actinomycetes found in soil [5]. Ivermectin is a safer and more potent semisynthetic product of two

avermectins. It is usually made up of 80% of 22,23-dihydroavermectin (B_{1a}) and 20% of 22,23-dihydroavermectin (B_{1b}) [6–8].

Despite being a promising antiparasitic drug, ivermectin has several non-ideal physico-chemical properties that can negatively impact its bioavailability. Firstly, the molecular weights of its B_{1a} and B_{1b} homologues are relatively large, at 875.1 and 861.1 g/mol, respectively [9, 10]. Ivermectin is also practically insoluble in water [11], with a reported aqueous solubility of around 4 µg/mL [12], and has a pK_a of 6.5 [13]. At a pH of 7.3 the octanol–water partition coefficient (log P) of ivermectin has been reported to be 3.2 [12]. Ivermectin is also classified as a biopharmaceutics classification system (BCS) class II drug [14–16].

Over the past few decades, an increasing amount of newly released active pharmaceutical ingredients (APIs) could either be classified as BCS class II or IV drugs [17]. It has been proposed that the decreased solubility, and permeability

✉ Hendrik J. R. Lemmer
righard.lemmer@nwu.ac.za

¹ Centre of Excellence for Pharmaceutical Sciences
(Pharmacen™), North-West University, Private Bag X6001,
Potchefstroom 2520, South Africa



in the case of class IV drugs, of newly released APIs can be linked to increases in molecular weights [18] and higher melting temperatures [19]. This has caused researchers to investigate new ways of increasing the bioavailability of large molecular weight APIs. Some of the techniques frequently employed in this regard are polymorphism screening and the preparation of co-crystals [20].

Crystals are usually created by inducing a change from a solution to a solid state [21]. When crystallization conditions are changed, the constituent molecules may pack in different patterns. This phenomenon is called polymorphism [22]. Changes in crystallization conditions include the use of different solvents or antisolvents, changes in stirring rates or the presence of impurities [23, 24]. A crystal has a melting point where the crystal lattice will break down because the constituent molecules have gained enough energy to overcome the attracting forces that hold the crystal together. Therefore, a higher melting point is usually indicative of a stronger crystal lattice and a lower dissolution rate [25]. Regarding polymorphism, the most stable form usually has the slowest dissolution rate, while also having the highest melting point [26–28].

Co-crystals are neutral, single-phase crystalline materials consisting of two or more molecules in stoichiometric ratios [21, 29]. These co-crystals can have enhanced physico-chemical properties compared to single component crystals, leading to improvements in stability, solubility, bioavailability and even the mechanical properties of APIs [21, 29–33]. Co-crystal preparation is also a way to improve the physico-chemical properties of an API without altering its molecular structure [30].

Avocado oil (AVO) and evening primrose oil (EPO) can be regarded as natural penetration enhancers with a high safety profile; these oils also have fatty acids leading to enhanced skin permeability [34–36]. Penetration enhancers can improve the fluidity of membrane structures, while also altering the skin's protective barrier, and possibly facilitate the solubility of APIs within the skin [37, 38]. Essential oils can be used to enhance the skin penetration of both hydrophilic and hydrophobic APIs [39, 40].

The main objective of this study was to prepare solid-state forms of ivermectin with enhanced oil solubility, with the goal of using these solids in future transdermal or topical drug delivery studies. There are several reasons why the transdermal or topical delivery of ivermectin might be advantageous. For instance, to minimize the risk of a possible Mazzotti-type reaction, an immune reaction to dead microfilariae experienced by some patients after oral ivermectin administration [41]. Topical administration can also achieve higher localization of an API in the skin [42]. This can be especially beneficial in the case of ivermectin, since it is also a P-glycoprotein substrate, and might therefore act like a BCS class IV API [43, 44]. For parasites located

deeper within the skin, topical treatment with ivermectin has already been shown to be more effective than oral administration [43]. Commercially, ivermectin is available as Sool-antra® 10 mg/g cream, for topical use.

By increasing the oil solubility, one should also be able to increase the drug loading capacity of micro- and nanoparticles and increase ivermectin concentrations in the oil phase of formulations. It was therefore decided to perform polymorphism and co-crystal screening studies of ivermectin with a non-ionic surface-active ingredient as co-former, since both co-crystals and different polymorphic forms have been known to increase the solubility of an API [21, 45, 46].

Materials and Methods

Materials

Ivermectin 86.8% (B_{1a}) $M = 875.1$ g/mol and 2.1% (B_{1b}) $M = 861.1$ g/mol, ivermectin reference standard (Sigma-Aldrich, MO, USA), avocado oil (AVO), evening primrose oil (EPO) (DB Fine Chemicals, Johannesburg, South Africa) and Span® 60 ($M = 430.62$ g/mol) (Sigma-Aldrich, MO, USA) were used as received. High performance liquid chromatography (HPLC) grade acetonitrile and methanol (ACE chemicals, Johannesburg, South Africa) were used for HPLC analyses.

Acetone, methanol (MeOH), ethanol (EtOH), dichloromethane (DCM), chloroform ($CHCl_3$), diethyl ether, ethyl acetate, propanol, 2-propanol, and 1-butanol (ACE chemicals, Johannesburg, South Africa) were used for polymorph screening. Sodium hydroxide (NaOH) and potassium dihydrogen phosphate (KH_2PO_4) were purchased from ACE Chemicals (Johannesburg, South Africa).

Polymorphism Screening

Supersaturated solutions of ivermectin were prepared in selected organic solvents. The mixtures were then covered with Parafilm® and stored in a cabinet until crystallization. The time-to-crystallization varied depending on the organic solvent used.

Co-processing

The method of liquid-assisted grinding was used to prepare the co-crystal candidates [21]. A mixture of ivermectin and Span® 60 was ground in a mortar and pestle at different molar ratios (ivermectin to Span® 60) of 3:1, 2:1 and 1:1, while slowly adding ethanol in small amounts until the desired consistency was obtained. The paste-like mixture was then allowed to dry overnight. The dried paste was then ground in a mortar and pestle to produce a fine white

powder. Three batches of each co-crystal candidate were prepared and tested for similarity using differential scanning calorimetry (DSC), thermogravimetric analysis (TGA) and X-ray powder diffraction (XRPD). The powder was stored in a desiccator over silica.

Physical mixtures of ivermectin and Span® 60 were also prepared, to serve as controls. For the physical mixtures, ivermectin and Span® 60 were ground and weighed individually. Thereafter, the powders were added to Falcon® tubes and vortexed (Heidolph Reax 2000, Heidolph, Schwabach, Germany) for 10 s to produce the physical mixtures. Three batches of each physical mixture were prepared and tested for similarity using DSC, TGA and XRPD. The powder mixtures were stored in a desiccator over silica.

Equilibrium Oil Solubility

An excess amount of ivermectin, the physical mixtures and the co-crystal candidates were suspended in AVO and EPO, respectively. It was determined that 1 g of powder and 5 mL of oil per Falcon® tube were sufficient to ensure oversaturated conditions. The Falcon® tubes were then vortexed for 1 min and submerged in a water bath at $32 \pm 2^\circ\text{C}$, fixed to a rotating axis (54 rpm) for 24 h. After 24 h, the Falcon® tubes were removed from the water bath and centrifuged at 1057 rcf (3000 rpm) for 5 min in an Eppendorf 5804 R centrifuge (Merck, Johannesburg, SA). The supernatant (ivermectin containing solution) was extracted using a syringe and filtered through a $0.45 \mu\text{m}$ Millipore® polyvinylidene difluoride (PVDF) membrane, whereafter 1 mL of this solution was diluted to 25 mL using ethanol and analyzed by HPLC. Six samples ($n=6$) of ivermectin, each physical mixture and co-crystal candidate, from different batches, were analyzed in each oil.

Thermal Analysis

Differential scanning calorimetry (DSC) was performed using a Mettler DSC 3+ (Mettler Toledo, Greifensee, Switzerland). The instrument was calibrated using zinc and indium standards. Sample powders of between 4 and 6 mg were accurately weighed into $40\text{-}\mu\text{L}$ aluminum pans. The pans were crimped and pinned before heating from 30 to 200°C with a heating rate of 10°C per min. Nitrogen gas flow was set to 20 mL/min. The thermograms were analyzed using Mettler STARe Default DB V14.00 software (V16.30a).

Thermogravimetric analysis (TGA) was performed using a Mettler DTG 3+ (Mettler Toledo, Greifensee, Switzerland). Calibration was done by using indium and zinc standards. Aluminum pans ($100 \mu\text{L}$) were used with sample powders of 4–6 mg. A nitrogen gas flow of 20 mL/min was used for all samples with a heating rate of 10°C per min over

a temperature range of 30 to 200°C . All thermograms were analyzed using Mettler STARe Default DB V14.00 software (V16.30a).

High Performance Liquid Chromatography (HPLC)

A Nexera-I LC-2040C 3D Plus (Shimadzu, Kyoto, Japan) equipped with a prominence communications bus module, degasser, liquid chromatograph, auto sampler, diode array detector and column oven was used to analyze all samples. A USP method [11] was subjected to in-house validation. A Venusil XBP C₁₈(2) $4.6 \times 250 \text{ mm}$, $5 \mu\text{m}$ (Agela Technologies, Ca, USA) column was used. The mobile phase was water:MeOH (13:87). The flow rate was set at 1.8000 mL/min with the column oven temperature set at 40°C . A stock solution was prepared with an ivermectin concentration of $4250.34 \mu\text{g/mL}$ in octanol. A series of seven dilutions were prepared within the range of $179.27\text{--}3400.27 \mu\text{g/mL}$. Each dilution was injected five times; all samples were first diluted in ethanol before analyzing. The retention time was 35 min (confirmed using the reference standard) with the theoretical limit of detection (LOD) and limit of quantification (LOQ) being $71.863 \mu\text{g/mL}$ and $217.768 \mu\text{g/mL}$, respectively. The calibration curve was linear, $R^2=0.9993$.

X-ray Powder Diffraction (XRPD)

XRPD analyses were performed using PANalytical Empyrean diffractometer (PANalytical, Almelo, Netherlands). The powder samples were ground in a mortar and pestle before being placed on a sample holder and flattened before analyzing. Data collector version 4.1 (4.1.0.25) was used to scan the samples. The measurement conditions were: target, Cu; voltage, 40 kV; current, 30 mA; divergence slit, 2.0 mm; antiscatter slit, 0.6 mm; detector slit, 0.2 mm; monochromator; scanning speed, $2^\circ/\text{min}$ (step size, 0.025° ; step time, 1.0 s). HighScore Plus version 3.0e (3.0.5) was used to examine the data.

Fourier-transform Infrared Spectroscopy (FTIR)

All samples were examined using a Shimadzu IR Tracer-100 spectrophotometer (Shimadzu, Kyoto, Japan). The samples were placed on a QATR 10 accessory and scanned 64 times over a range of $400\text{--}4000 \text{ cm}^{-1}$. The data was then processed using LabSolutions version 1.108.

Octanol-buffer Partition Coefficient (log P)

Equal parts of octanol and buffer (PBS pH 7.4) were measured and allowed to mix for 24 h. This allowed the phases to become saturated with each other before starting the experiment. The mixture of octanol and buffer was then left to separate in a separating funnel. Roughly 2.0 h

was required for the phases to be properly separated. An oversaturated amount of ivermectin (1 g) was weighed in a Falcon® tube, whereafter 5 mL of the buffer phase was added and submerged in a water bath ($32 \pm 2^\circ\text{C}$) fixed to a rotating axis (54 rpm) for 45 min. The octanol phase, 5 mL, was added to the Falcon® tube and placed back in the water bath for 2.5 h. The Falcon® tubes were then centrifuged with an Eppendorf 5804 R centrifuge for 5 min at 2057 rcf (3000 rpm). The bottom phase in the Falcon® tube was the buffer phase. The buffer phase was undiluted and filtered before analyzing on the HPLC. The top (octanol) phase was diluted 1 mL to 100 mL with ethanol. The diluted octanol was filtered before HPLC analyses. The experiment was done in triplicate and repeated with the different molar ratios of ivermectin:Span® 60 in 3:1, 2:1 and a 1:1.

Preparation of Structures for Molecular Docking

The IVM crystal surface representations were constructed using Mercury CSD 2023.3.1 [47] and single crystal data of

refcode BIFYOF found in the Cambridge Crystallographic Data Centre (CCDC). Crystal surfaces were constructed along the a, b and c axes of the unit cell. BIFYOF was chosen for this study because of the similarities between its calculated powder diffraction pattern (Fig. S1 in supplementary information) and the experimental diffractograms obtained in this study (Figs. 1 and 2). The different surface representations were then saved in.pdb format for further processing.

The chemical structure of Span® 60 was downloaded from PubChem in SDF format and converted to.pdb format using PyMOL [48].

Processing of Structures for Molecular Docking

The crystal surfaces (receptors) and Span® 60 (ligand) were processed using MGLTools-1.5.7 (The Scripps Research Institute, La Jolla, CA, USA) prior to docking. The molecular structure of Span® 60 was read using the “Ligand” button, its torsion root detected, and saved in PDBQT format. The crystal surfaces were opened individually, and polar

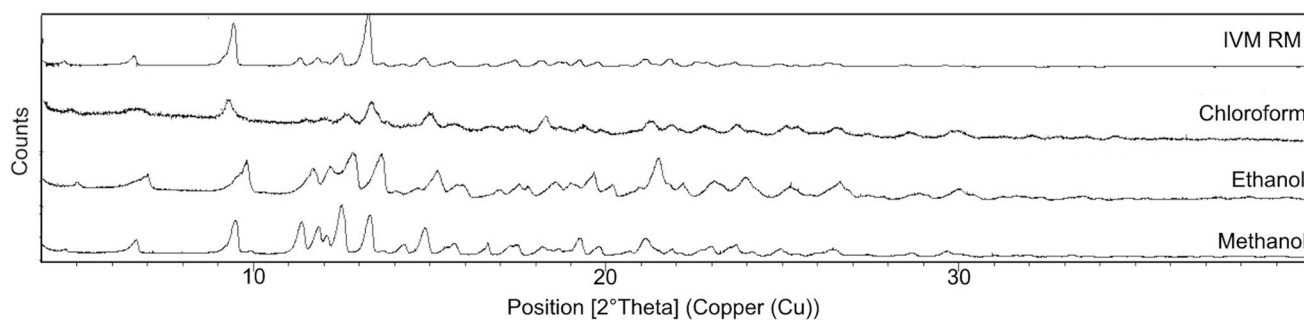


Fig. 1 XRPD diffractograms of ivermectin raw material and the crystals obtained from recrystallization in chloroform, ethanol, and methanol, respectively

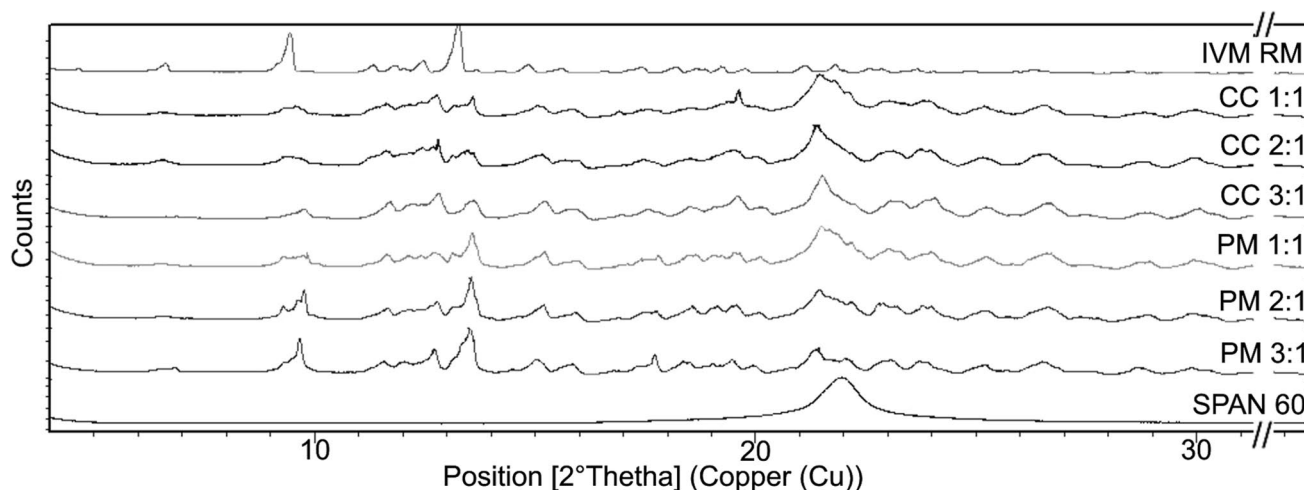


Fig. 2 XRPD diffractograms of ivermectin raw material (RM), co-crystal candidates (CC), physical mixtures (PM) and Span® 60

hydrogens were added. The surfaces were chosen as macromolecules and saved in PDBQT format. Blind docking was performed to allow the software to calculate the most energetically favorable binding locations for Span® 60 on the crystal surfaces. This was done by drawing grid boxes to completely cover each crystal surface. The grid box dimensions and centers were then used in the *config* files of each surface's molecular docking run.

Molecular Docking

Molecular docking was performed using AutoDock Vina 1.2 (The Scripps Research Institute, La Jolla, CA, USA) [49]. The binding affinities of the nine best models can be found in Table S1 (Supplementary information). Molecular interactions of the different binding models were analyzed using MGLTools-1.5.7.

Statistical Analyses

To statistically evaluate the solubility enhancements of the proposed co-crystal candidates over their respective physical mixtures and ivermectin raw material, pair-wise comparisons were performed. Since the sample sizes were relatively small ($n=6$), pair-wise Mann–Whitney U tests were performed with Bonferroni adjustments of the p values. All statistical analyses were done using Python 3.9 [50] and the Statsmodels library [51]. Data storage and handling from Excel were performed using the Pandas library [52], while vectorized computations were performed using the NumPy library [53]. Figures were created using the Matplotlib [54] and Seaborn [55] libraries.

Results and Discussion

The first step in attempting to find a solid-state form of ivermectin with enhanced oil solubility was to perform a polymorphism screening. XRPD diffractograms of the crystals obtained from recrystallization are presented in Fig. 1. The peak positions on the diffractograms of the crystals obtained from chloroform and methanol were similar to those of ivermectin raw material. Although the diffractogram of the crystals obtained from ethanol appeared to be different, closer inspection revealed that the raw material's peaks were still present but shifted to the right. This could simply be due to a denser molecular packing within these crystals. The results of the polymorphism screening therefore suggest that, under the conditions in our laboratory, new polymorphs of ivermectin could not be prepared. This inability to obtain new polymorphs can possibly be explained by the results presented by Shubin *et al.* [56], in a recent paper where they prepared solvates of ivermectin with ethanol,

γ -valerolactone (GVL) and methyl *tert*-butyl ether (MTBE). Their single crystal X-ray diffraction (SXRD) data showed that the structural conformation of ivermectin was largely retained in all three solvates. This general conformation of ivermectin was also consistent with that of an ivermectin acetone-CHCl₃ solvate, BIFYOF, which had previously been deposited on the Cambridge Crystallographic Data Centre (CCDC), and with the structure generated from density function theory (DFT) calculations [56]. Shubin *et al.* further found that the different solvents mainly determined the space groups, and crystal structures, of their solvates, while the crystal frameworks were stabilized by interactions between neighboring ivermectin molecules. This preference of ivermectin to take on a general conformation can limit the number of packing options ivermectin has inside the crystal lattice and can explain the difficulty in obtaining new polymorphs encountered in this study.

During the equilibrium solubility studies it was observed that ivermectin raw material, and its recrystallization products, were poorly “wetttable” in AVO and EPO, i.e., it either floated on top of the oils or remained at the bottom of the Falcon® tubes in dry clumps. It was therefore decided to attempt to address the wettability problem, as this might also improve the oil solubility of ivermectin. Since one of the study's requirements was that the final product be a solid, it was decided to attempt to prepare co-crystals of ivermectin with a suitable co-former. The co-former had to be able to address the wettability problem and be freely soluble in oils. Therefore, Span® 60 was chosen since it is a solid at room temperature, is a non-ionic surfactant and is lipophilic.

XRPD diffractograms of the co-crystal candidates, physical mixtures and individual components are presented in Fig. 2. The diffractograms of the co-crystal candidates were very similar to those of their respective physical mixtures. However, small differences could still be observed, e.g., at 9.6 and 17.7°2 θ there were peaks visible in the physical mixtures that could not be found in the co-crystal candidates. These peaks were also not present in ivermectin raw material. Apart from these differences, the diffractograms of the co-crystal candidates and their respective physical mixtures were very similar. It should be noted here that Span® 60 is not crystalline, as is evident by its diffuse halo in Fig. 2. This suggests that the peak positions were mostly influenced by the crystal packing of ivermectin, an observation that was consistent with the previously mentioned findings by Shubin *et al.* regarding the dominant role of neighboring ivermectin molecules in stabilizing the crystal structure [56]. It is possible that the intermolecular interactions between ivermectin and Span® 60, in both the co-crystal candidates and physical mixtures, were not only very similar, but also very limited. To investigate this, FTIR spectra of ivermectin raw material, Span® 60, the co-crystal candidates and physical mixtures were compared to each other.

The FTIR spectra are presented in Fig. 3. Like the XRPD diffractograms, the FTIR spectra of the physical mixtures and co-crystal candidates were almost similar. Considering the chemical structures of ivermectin and Span® 60, the lack of traditional hydrogen bond acceptors is immediately apparent, with both compounds exhibiting only one carbonyl oxygen. However, both ivermectin and Span® 60 have several hydroxyl groups. Therefore, the hydroxyl (–OH) band region of the FTIR spectra is of particular interest. In this region (3250–3500 cm^{-1}) the spectra of the physical mixtures and co-crystal candidates correspond to that of ivermectin raw material (IVM RM). However, the broad –OH peak of Span® 60 is no longer visible in the physical mixtures and co-crystal candidates, suggesting that all of Span® 60's –OH groups underwent interactions with ivermectin, while ivermectin's –OH groups remained unchanged. The difference between the spectra of the co-crystal candidates and physical mixtures can be found in the alkyl chain band region (2800–2950 cm^{-1}). In this region, the peaks of the physical mixtures were again identical to that of IVM RM. However, for the co-crystal candidates, this region corresponded to the peaks of Span® 60's alkyl chain (highlighted in Fig. 3), with some ivermectin alkyl peaks appearing in the 3:1 ratio co-crystal candidate (which contains one molecule Span® 60

for every three ivermectin molecules). The results therefore suggest that, while the intermolecular interactions between ivermectin and Span® 60 in the co-crystal candidates and physical mixtures were strikingly similar, there was a difference between these solids. The complete absence of Span® 60's functional groups in the physical mixtures suggests that it was completely dispersed between the ivermectin crystals (powder). However, in the co-crystal candidates, the Span® 60 molecules were orientated in such a way that their alkyl chains were “freer” (could absorb IR radiation and stretch more readily), while the hydrophilic “heads” of the molecules underwent interactions with ivermectin. This small difference in intermolecular interactions could explain why the XRPD diffractograms were also mostly similar. Since a co-crystal should be a homogeneous (single-phase) system, this was tested using thermal analyses.

DSC thermograms of the different solids tested in this study are presented in Fig. 4. Span® 60 is a non-ionic surfactant with a phase-transition temperature (T_c) of around 54°C (Fig. 4a). Since the endothermal event associated with this phase transition is the result of a conformation change in the surfactant's alkyl chain [57–59], it is reasonable to assume that this endothermal event will be present in all the thermograms of solids containing Span® 60. From Fig. 4,

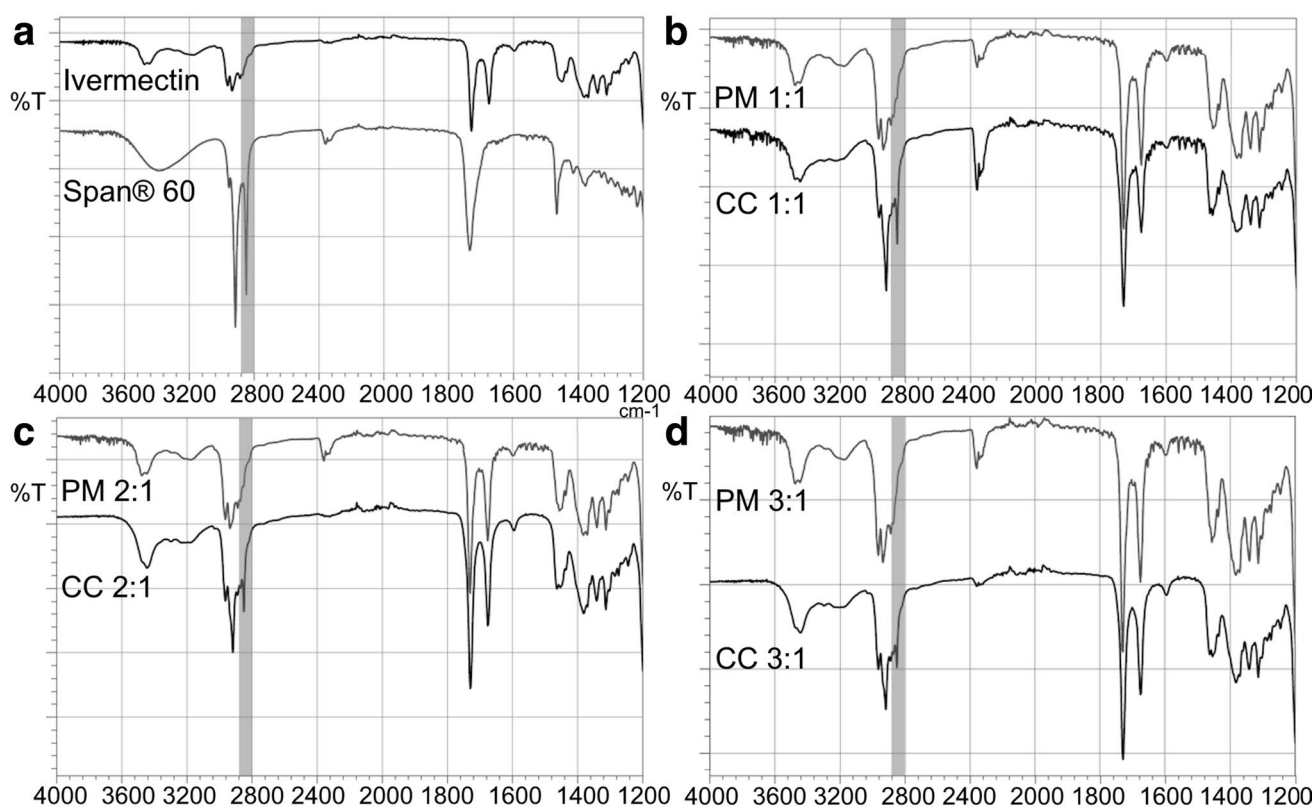


Fig. 3 FTIR spectra of **a** ivermectin raw material and Span® 60, **b** the 1:1, **c** 2:1 and **d** 3:1 ivermectin:Span® 60 molar ratio physical mixtures (PM) and co-crystal candidates (CC)

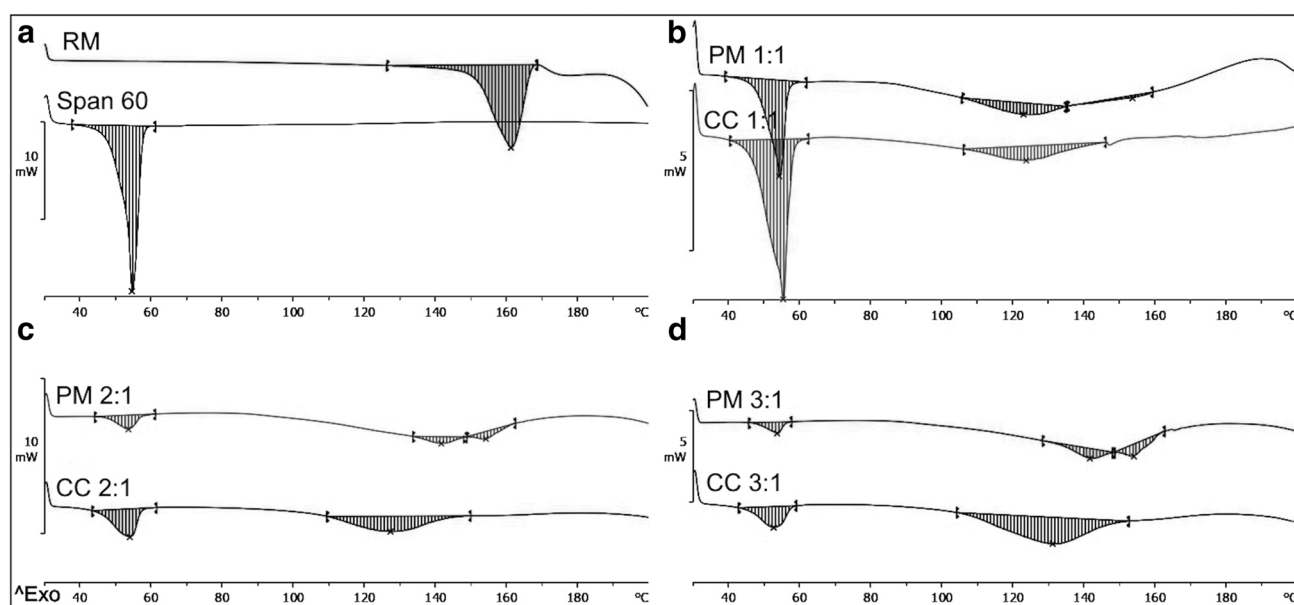


Fig. 4 DSC thermograms of **a** ivermectin raw material (RM) and Span® 60, **b** the 1:1, **c** 2:1 and **d** 3:1 ivermectin:Span® 60 molar ratio physical mixtures (PM) and co-crystal candidates (CC)

it is observed that this was indeed the case. A correlation with the FTIR data, which suggested that Span® 60's alkyl chains were freer in the co-crystal candidates than in the physical mixtures, can be seen in Fig. 4, with consistently larger alkyl chain conformation change enthalpies (areas under the curve) for the co-crystal candidates compared to their physical mixture counterparts. Apart from the alkyl chains' conformation change, all the co-crystal candidates displayed only one melting point, while the physical mixtures presented with two. Details on the melting points can be found in Table I.

The data in Table I suggests that the melting points of the co-crystal candidates, and first melting points of the physical mixtures, were all well below that of ivermectin raw material. For the physical mixtures, the second melting points were also below the melting point of ivermectin. Except for the 1:1 molar ratio physical mixture and co-crystal candidate, all the co-crystal candidates displayed melting points more than 10 °C below the first melting points of the physical mixtures. Usually, one would expect a co-crystal's melting point to lie between the melting points of the API and co-former. However, since Span® 60 is not crystalline (Fig. 2) and does not have a melting point in the traditional sense, this co-crystal behavior could not be confirmed. It was observed though that the melting points of the co-crystal candidates increased, i.e., moved closer to the melting point of ivermectin raw material, with an increase in the amount of ivermectin molecules present. This observation at least corresponds to the melting point behavior expected from co-crystals. However, in the absence of SXRD data,

the preparation of co-crystals could not be confirmed, and therefore the co-crystal candidates will be referred to as co-processed crystalline solids.

Collating the XRPD, FTIR and DSC data, possible explanations for the observations can again be found in the work presented by Shubin *et al.* Combining their findings regarding the conformation of ivermectin and its dominant role in stabilizing the crystals' structures, Shubin *et al.* concluded that monoclinic ivermectin crystals were examples of host–guest type systems [56]. This was a direct result of ivermectin's inability to pack efficiently, because of the *crown*-formation its molecular structure adopted, leaving voids inside the crystals. Orthorhombic ivermectin crystals also displayed voids in their crystal structures, albeit larger than those in the monoclinic crystals. The volumes of these voids were found to be 82 and 221 Å³, and 552 Å³ for the monoclinic and orthorhombic crystals, respectively. Therefore, molecules can fit into these voids if they are the correct size [56]. It is possible that co-processing of ivermectin with Span® 60, using the liquid-assisted grinding technique, resulted in the hydrophilic heads of the Span® 60 molecules filling the cavities these voids would leave on the surface of the ivermectin crystals.

To investigate this hypothesis, blind molecular docking studies were performed using Span® 60 as ligand and the surfaces of an IVM crystal (CCDC refcode BIFYOF) as receptors. The binding affinities of the different models, and figures of the intermolecular interactions, can be found in the supplementary information. For all the proposed interaction models the highest binding affinities were observed

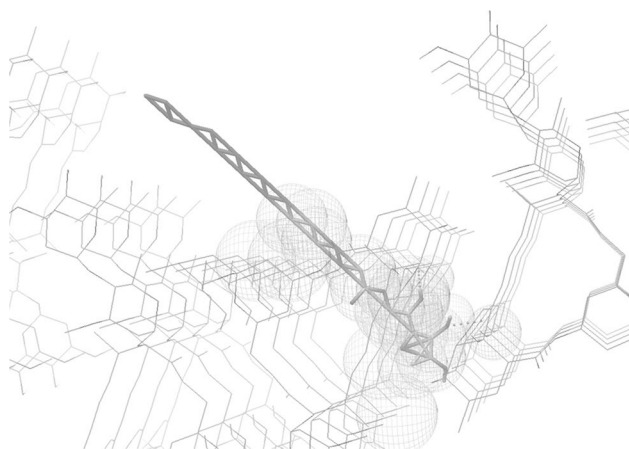


Fig. 5 Molecular docking results showing a Span® 60 molecule with its hydrophilic head embedded in a cavity on the simulated surface of an IVM crystal. Close contact interactions are shown as spheres and hydrogen bonds as dotted lines

Table I Phase Transition and Melting Point Data for Ivermectin, Span® 60, Physical Mixtures (PM) and Co-crystal Candidates (CC) Tested

	Span® 60 phase transition (°C)	Melting point 1 (°C)	Melting point 2 (°C)
Ivermectin	-	161.33	-
Span® 60	55.17	-	-
PM 1:1	54.36	123.06	153.74
CC 1:1	54.13	125.83	-
PM 2:1	53.76	141.02	154.36
CC 2:1	54.06	127.37	-
PM 3:1	53.77	141.69	154.02
CC 3:1	52.74	131.33	-

where interactions took place between the hydrophilic head of Span® 60 and IVM. Most of the interactions were close contact interactions, i.e., atoms closer than the sum of their van der Waals radii. However, some hydrogen bonding interactions were also observed, as presented here in Fig. 5. The proposed model in Fig. 5 is in line with the observations made previously concerning the FTIR spectrum and thermal analysis data. The model presented in Fig. 5, as well as the other models in the supplementary information, suggests that it is possible for Span® 60 to fill cavities on the surface of IVM crystals. Since this does not change the underlying

crystal structure, but rather “coats” it, these type of surface interactions could explain why the characteristic peaks of IVM were still visible in the XRPD diffractograms of the co-processed solids.

Thermogravimetric analysis showed that both ivermectin and Span® 60 had average mass losses of about 4.5% (4.64 and 4.46%, respectively). For the 1:1 molar ratio, the average mass losses of both the physical mixture and co-processed solids were 6% (5.9983% and 6.0036%, respectively). Similarly, for the 2:1 ratio physical mixture and co-processed solids the average mass losses were 9% (9.0971% and 8.9593%, respectively). The same was true for the 3:1 molar ratio physical mixture and co-processed solids, which had an average mass loss of 7% (6.7884% and 7.2234%, respectively). The thermogravimetric results therefore suggest that mass loss was independent of solid-state form but varied based on the molar ratios of the constituent molecules.

In this study, the measured log *P* value of ivermectin was 3.001 ± 0.012 ($n=3$), which was comparable to the literature value of 3.2 [12]. The measured log *P* values of the physical mixtures and co-processed solids are presented in Table II. The results showed that for the 1:1 and 2:1 molar ratios, the log *P* values of the physical mixtures and co-processed solids, respectively, were close to one another. For the 3:1 molar ratio, the log *P* value of the co-processed solids was higher than that of the physical mixture. For the co-processed solids, the log *P* values increased with an increase in the amount of ivermectin molecules present.

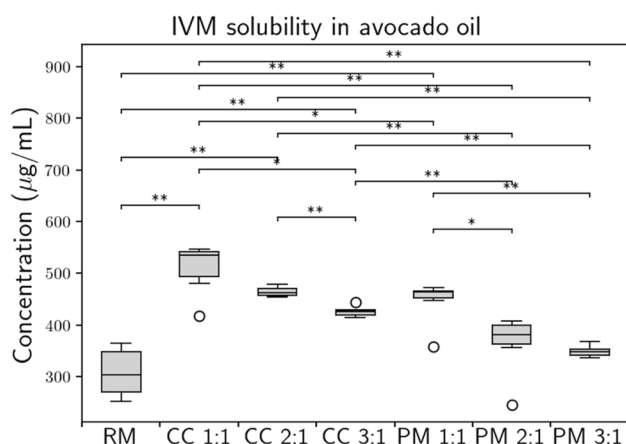
Results of the equilibrium (24 h) oil solubility studies in AVO and EPO are presented in Table III. The physical mixtures and co-processed solids all displayed improvements in solubility compared to ivermectin raw material. The statistical analysis of the solubility studies showed that the differences in AVO solubility between the raw material and 2:1 and 3:1 physical mixtures were not significant (Fig. 6). However, in EPO all the physical mixtures and co-processed solids showed significant improvements in solubility over the raw material. The largest improvement in AVO solubility was seen with the 1:1 molar ratio co-processed solids, while the largest improvement in EPO solubility was seen with the 2:1 co-processed solids (Table III). Statistical analysis also showed that, in AVO, the 1:1 molar ratio co-processed solids’ solubility differed significantly from all the other groups, with the exception of the 2:1 co-processed solids (Fig. 6), while in EPO the 2:1 co-processed solids’ solubility differed from that of most groups, with the exceptions being the 3:1 co-processed solids and 3:1 physical mixture (Fig. 7).

Table II Log *P* Values of the Physical Mixtures (PM) and Co-Crystal Candidates (CC) in Different Molar Ratios

1:1		2:1		3:1	
PM	CC	PM	CC	PM	CC
2.84 ± 0.07	2.87 ± 0.07	3.16 ± 0.08	3.02 ± 0.13	3.08 ± 0.06	3.34 ± 0.04

Table III Equilibrium Solubility Values (Mean \pm std) of Ivermectin Raw Material, Physical Mixtures (PM) and Co-Crystal Candidates (CC) in AVO and EPO ($n=6$ in Each Oil)

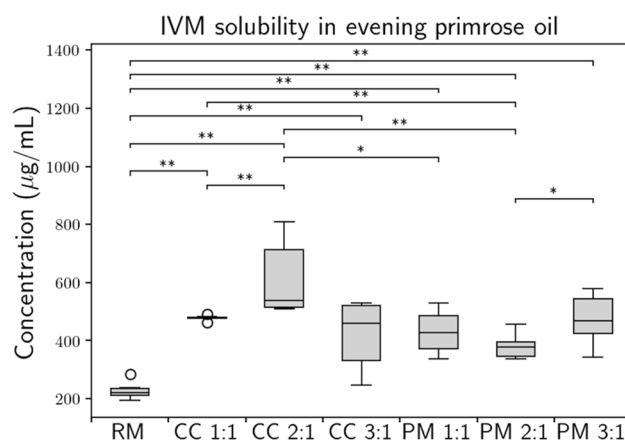
Solubility	Ivermectin	1:1		2:1		3:1	
		PM	CC	PM	CC	PM	CC
AVO	307.5 \pm 47.55	445.51 \pm 43.68	509.72 \pm 51.53	362.57 \pm 60.25	464.27 \pm 9.82	349.20 \pm 11.59	426.09 \pm 10.46
EPO	228.06 \pm 31.23	429.78 \pm 76.29	478.39 \pm 9.65	380.88 \pm 44.79	612.72 \pm 137.95	473.21 \pm 89.95	421.53 \pm 122.57

**Fig. 6** Boxplots and statistical significance indicators of IVM's solubility in avocado oil (AVO). The groups consist of IVM raw material (RM), co-crystal candidates (CC) and physical mixtures (PM) in different molar ratios. For the significance indicators, * indicates significant differences ($p \leq 0.05$) and ** indicates very significant differences ($p \leq 0.01$)

The solubility results therefore suggest that, in both AVO and EPO, at least one co-processed solid displayed a significant improvement in oil solubility compared to the raw material and the physical mixtures, with the only exception being the 3:1 physical mixture in EPO.

In recent years, several studies have attempted to improve the solubility of ivermectin, either through hydroxypropyl- β -cyclodextrin (HP- β -CD) complexation [59], or the preparation of nanocrystals [42, 44]. However, these studies were focused on improving the aqueous solubility of ivermectin. To the best of the authors' knowledge, this study represents the first attempt to improve the oil solubility of ivermectin. The results presented here showed that, in AVO the 1:1 molar ratio co-processed solid was able to improve ivermectin's solubility by 66%, and in EPO the 2:1 co-processed solid improved ivermectin's solubility by 169%.

A possible explanation for why the co-processed solids outperformed the physical mixtures can be found in our hypothesis that co-processing resulted in Span® 60's hydrophilic head groups to occupy cavities on the surface of the ivermectin crystals, effectively coating the crystals with Span® 60. These structures could result in better oil "wettability" than that obtained from normal powder mixtures, leading to better

**Fig. 7** Boxplots and statistical significance indicators of IVM's solubility in evening primrose oil (EPO). The groups consist of IVM raw material (RM), co-crystal candidates (CC) and physical mixtures (PM) in different molar ratios. For the significance indicators, * indicates significant differences ($p \leq 0.05$) and ** indicates very significant differences ($p \leq 0.01$)

solubility. However, this hypothesis will first need to be thoroughly investigated, and will be left as a future prospect.

Conclusion

This study attempted to improve the oil solubility of ivermectin through solid-state modifications. The rationale behind attempting to improve oil solubility was to investigate techniques that can be used to increase drug loading in lipid-based dosage forms and possibly micro- and/or nanoparticles prepared from oil-in-water emulsions. The initial polymorph screening proved inconclusive, and the resulting crystals could not improve ivermectin's solubility in AVO and EPO. During the initial equilibrium solubility studies, it was observed that ivermectin was poorly wettable in AVO and EPO, with the powder remaining either on top of or below the oils in dry clumps. Attempts were made to prepare co-crystals of ivermectin with a lipid-soluble non-ionic surfactant as co-former, to address the wettability issues and possibly improve oil solubility. For this study, Span® 60 was chosen as co-former.

The XRPD and FTIR results showed only small differences between the co-crystal candidates and their physical

mixture counterparts. However, the FTIR spectra of the co-crystal candidates showed the presence of Span® 60's alkyl chain peaks, which were absent in the spectra of the physical mixtures. This suggested that co-processing of ivermectin and Span® 60 using the liquid-assisted grinding technique resulted in crystalline solids where the alkyl chains of Span® 60 had more freedom compared to the physical mixtures. The DSC thermograms suggested that the co-crystal candidates were homogenous (single-phase) systems compared to the physical mixtures, since, apart from the initial endotherms resulting from conformation changes in Span® 60's alkyl chains, the co-crystal candidates presented with only one melting endotherm, while the physical mixtures all displayed two melting endotherms. Apart from the 1:1 co-crystal, the melting points of the co-crystal candidates were all lower than the lowest melting points of the physical mixtures. However, without SXRD data, the successful preparation of co-crystals could not be confirmed. Therefore, the co-crystal candidates should rather be referred to as co-processed crystalline solids.

The presence of Span® 60 improved the solubility of ivermectin in EPO and AVO, as it was able to address the wettability issue. The co-processed solids were able to improve the solubility of ivermectin even beyond that obtained from the physical mixtures, with the 1:1 molar ratio co-processed solid improving ivermectin's solubility by 66% in AVO, and the 2:1 co-processed solid improving ivermectin's solubility by 169% in EPO. Therefore, these co-processed solids represent a promising solid-state modification that can be used in future studies to increase ivermectin loading in oil-based dosage forms.

Supplementary Information The online version contains supplementary material available at <https://doi.org/10.1208/s12249-024-02783-0>.

Acknowledgements The authors would like to express their gratitude towards Madelein Geldenhuys for her guidance during HPLC method validation.

Author Contribution All authors contributed equal amounts to the article. This study was conceptualized and designed by Luandri de Vos, Wilna Liebenberg and Righard Lemmer. The experiments and data analyses were performed by Luandri de Vos, Wilna Liebenberg, Anita Wessels, Madelein Geldenhuys and Righard Lemmer. The manuscript was written and edited by Luandri de Vos, Wilna Liebenberg, Minja Gerber, Anita Wessels and Righard Lemmer. Wilna Liebenberg, Minja Gerber, Anita Wessels and Righard Lemmer supervised the project, and Minja Gerber attained funding. All authors reviewed the manuscript and approved the final version.

Funding Open access funding provided by North-West University. The authors would like to express their gratitude towards the financial support of the National Research Foundation (NRF) of South Africa: Competitive Programme for Rated Researchers (CPRR) (Grant no. 141957). Any opinions, findings, conclusions or recommendations expressed in this material are those of the authors, and therefore the NRF does not accept any liability with regard thereto.

Declarations

Conflict of Interest The authors declare no competing interests.

Open Access This article is licensed under a Creative Commons Attribution 4.0 International License, which permits use, sharing, adaptation, distribution and reproduction in any medium or format, as long as you give appropriate credit to the original author(s) and the source, provide a link to the Creative Commons licence, and indicate if changes were made. The images or other third party material in this article are included in the article's Creative Commons licence, unless indicated otherwise in a credit line to the material. If material is not included in the article's Creative Commons licence and your intended use is not permitted by statutory regulation or exceeds the permitted use, you will need to obtain permission directly from the copyright holder. To view a copy of this licence, visit <http://creativecommons.org/licenses/by/4.0/>.

References

1. Laing R, Gillan V, Devaney E. Ivermectin—old drug, new tricks? *Trends Parasitol.* 2017;33(6):463–72. <https://doi.org/10.1016/j.pt.2017.02.004>.
2. Van Voorhis WC, Hooft van Huijsduijnen R, Wells TNC. Profile of William C. Campbell, Satoshi Ōmura, et al. 2015 Nobel laureates in physiology or medicine. *Proc Natl Acad Sci USA.* 2015;112(52):15773–6. <https://doi.org/10.1073/pnas.1520952112>.
3. Sharun K, Shyamkumar TS, Aneesha VA, Dhama K, Pawde AM, Pal A. Current therapeutic applications and pharmacokinetic modulations of ivermectin. *Vet World.* 2019;12(8):1204–11. <https://doi.org/10.14202/vetworld.2019.1204-1211>.
4. Machado M, Dantas IL, Galvão JG, Lima AD, da Cunha Gonsalves JK, Almeida ED, et al. Microemulsion systems to enhance the transdermal permeation of ivermectin in dogs: a preliminary in vitro study. *Res Vet Sci.* 2020;133:31–8. <https://doi.org/10.1016/j.rvsc.2020.08.009>.
5. El-Saber Batiha G, Alqahtani A, Ilesanmi OB, Saati AA, El-Mleeh A, Hetta HF, et al. Avermectin derivatives, pharmacokinetics, therapeutic and toxic dosages, mechanism of action, and their biological effects. *Pharmaceuticals.* 2020;13(8):196. <https://doi.org/10.3390/ph13080196>.
6. Crump A. Ivermectin: Enigmatic multifaceted “wonder” drug continues to surprise and exceed expectations. *J Antibiot (Tokyo).* 2017;70(5):495–505.
7. Canga AG, Prieto AMS, Diez Liébana MJ, Martínez NF, Sierra Vega M, García Vieitez JJ. The pharmacokinetics and interactions of ivermectin in humans—a mini-review. *AAPS J.* 2008;10(1):42–6. <https://doi.org/10.1208/s12248-007-9000-9>.
8. Tang M, Hu X, Wang Y, Yao X, Zhang W, Yu C, et al. Ivermectin, a potential anticancer drug derived from an antiparasitic drug. *Pharmacol Res.* 2021;163: 105207. <https://doi.org/10.1016/j.phrs.2020.105207>.
9. Weil M, Scholz S, Zimmer M, Sacher F, Duis K. Gene expression analysis in zebrafish embryos: a potential approach to predict effect concentrations in the fish early life stage test. *Environ Toxicol Chem.* 2009;28(9):1970–8. <https://doi.org/10.1897/08-627.1>.
10. Ashour DS. Ivermectin: from theory to clinical application. *Int J Antimicrob Agents.* 2019;54(2):134–42. <https://doi.org/10.1016/j.ijantimicag.2019.05.003>.
11. USP. Ivermectin Tablets [Internet]. USP41-NF36. 2022 [cited 2022 Mar 28]. Available from: <https://online.uspnf.com/uspnf/>

- [document/1_GUID-740FA3F1-EB36-4E5C-8DD2-8C9D6DA81F43_1_en-US](#)
12. Liebig M, Fernandez ÁA, Blübaum-Gronau E, Boxall A, Brinke M, Carbonell G, et al. Environmental risk assessment of ivermectin: a case study. *Integr Environ Assess Manag*. 2010;6(SUPPL. 1):567–87. <https://doi.org/10.1002/ieam.96>.
 13. Rolim LA, Dos Santos FC, Chaves LL, Gonçalves ML, Freitas-Neto JL, Da Silva do Nascimento AL, et al. Preformulation study of ivermectin raw material. *J Therm Anal Calorim*. 2015;120(1):807–16. <https://doi.org/10.1007/s10973-014-3691-9>.
 14. Raman S, Polli JE. Prediction of positive food effect: bioavailability enhancement of BCS class II drugs. *Int J Pharm*. 2016;506(1–2):110–5. <https://doi.org/10.1016/j.ijpharm.2016.04.013>.
 15. Verma S, Patel U, Patel RP. Formulation and evaluation of ivermectin solid dispersion. *J Drug Deliv Ther*. 2017;7(7):15–7. <https://doi.org/10.22270/jddt.v7i7.1572>.
 16. Camargo JA, Sapin A, Nouvel C, Daloz D, Leonard M, Bonneaux F, et al. Injectable PLA-based in situ forming implants for controlled release of Ivermectin a BCS Class II drug: solvent selection based on physico-chemical characterization. *Drug Dev Ind Pharm*. 2013;39(1):146–55. <https://doi.org/10.3109/03639045.2012.660952>.
 17. Wang K, Sun CC. Crystal Growth of celecoxib from amorphous state: polymorphism, growth mechanism, and kinetics. *Cryst Growth Des*. 2019;19(6):3592–600.
 18. Thorat YS, Gonjari ID, Hosmani AH. Solubility enhancement techniques: a review on conventional and novel approaches. *Int J Pharm Sci Res*. 2011;2(10):2501–13.
 19. Zografi G, Newman A. Introduction to amorphous solid dispersions. In: Newman A, editor. *Pharmaceutical amorphous solid dispersions*. Lafayette, Indiana USA: Wiley & Son; 2015. pp. 1–41.
 20. Ghadi R, Dand N. BCS class IV drugs: highly notorious candidates for formulation development. *J Control Release*. 2017;248:71–95. <https://doi.org/10.1016/j.jconrel.2017.01.014>.
 21. Karimi-Jafari M, Padrela L, Walker GM, Croker DM. Creating cocrystals: a review of pharmaceutical cocrystal preparation routes and applications. *Cryst Growth Des*. 2018;18(10):6370–87. <https://doi.org/10.1021/acs.cgd.8b00933>.
 22. Sun Y, Xi H, Chen S, Ediger MD, Yu L. Crystallization near glass transition: transition from diffusion-controlled to diffusionless crystal growth studied with seven polymorphs. *J Phys Chem B*. 2008;112(18):5594–601. <https://doi.org/10.1021/jp7120577>.
 23. Benmessaoud I, Koutchoukali O, Bouhelassa M, Nouar A, Veesler S. Solvent screening and crystal habit of metformin hydrochloride. *J Cryst Growth*. 2016;451:42–51. <https://doi.org/10.1016/j.jcrysgro.2016.07.001>.
 24. Gu CH, Young V Jr, Grant DJ. Polymorph screening: influence of solvents on the rate of solvent-mediated polymorphic transformation. *J Pharm Sci*. 2001;90(11):1878–90. <https://doi.org/10.1002/jps.1137>.
 25. Dorgham EM, El Maghraby GM, Essa EA, Arafa MF. Melting point depression for enhanced dissolution rate of eslicarbazepine acetate. *Drug Dev Ind Pharm*. 2023;48(12):717–26. <https://doi.org/10.1080/03639045.2022.2162074>.
 26. Bauer JF. Polymorphism-A critical consideration in pharmaceutical development, manufacturing, and stability. *J Valid Technol*. 2008;14(5):15–24.
 27. Byrn SR, Pfeiffer RR, Stowell J. *Solid-state chemistry of drugs*. 2nd ed. West Lafayette, Indiana: SSCI Inc; 1999.
 28. Vippagunta SR, Brittain HG, Grant DJW. Crystalline solids. *Adv Drug Deliv Rev*. 2001;48(1):3–26. [https://doi.org/10.1016/S0169-409X\(01\)00097-7](https://doi.org/10.1016/S0169-409X(01)00097-7).
 29. Berry DJ, Steed JW. Pharmaceutical cocrystals, salts and multicomponent systems; intermolecular interactions and property based design. *Adv Drug Deliv Rev*. 2017;117:3–24. <https://doi.org/10.1016/j.addr.2017.03.003>.
 30. Kuminek G, Cao F, de Oliveira Bahia, da Rocha A, Gonçalves Cardoso S, Rodríguez-Hornedo N. Cocrystals to facilitate delivery of poorly soluble compounds beyond-rule-of-5. *Adv Drug Deliv Rev*. 2016;101:143–66. <https://doi.org/10.1016/j.addr.2016.04.022>.
 31. Wu W, Wang Y, Löbmann K, Grohgan H, Rades T. Transformations between co-amorphous and co-crystal systems and their influence on the formation and physical stability of co-amorphous systems. *Mol Pharm*. 2019;16(3):1294–304. <https://doi.org/10.1021/acs.molpharmaceut.8b01229>.
 32. Schultheiss N, Newman A. Pharmaceutical cocrystals and their physicochemical properties. *Cryst Growth Des*. 2009;9(6):2950–67. <https://doi.org/10.1021/cg900129f>.
 33. Karki S, Friščić T, Fabián L, Laity PR, Day GM, Jones W. Improving mechanical properties of crystalline solids by cocrystal formation: new compressible forms of paracetamol. *Adv Mater*. 2009;21(38–39):3905–9. <https://doi.org/10.1002/adma.200905333>.
 34. Viljoen JM, Cowley A, Preez J, Gerber M, Plessis J. Penetration enhancing effects of selected natural oils utilized in topical dosage forms. *Drug Dev Ind Pharm*. 2015;41(12):2045–54. <https://doi.org/10.3109/03639045.2015.1047847>.
 35. Aggarwal S, Agarwal S, Jalhan S. Essential oils as novel human skin penetration enhancer for transdermal drug delivery: a review. *Int J Pharma Bio Sci*. 2013;4(1):857–68.
 36. Fox LT, Gerber M, Du Plessis J, Hamman JH. Transdermal drug delivery enhancement by compounds of natural origin. *Molecules*. 2011;16(12):10507–40. <https://doi.org/10.3390/molecules161210507>.
 37. Walker RB, Smith EW. The role of percutaneous penetration enhancers. *Adv Drug Deliv Rev*. 1996;18(3):295–301. [https://doi.org/10.1016/0169-409X\(95\)00078-L](https://doi.org/10.1016/0169-409X(95)00078-L).
 38. Louw EV, Liebenberg W, Willers C, Dube A, Aucamp ME, Gerber M. Comparative study on the topical and transdermal delivery of diclofenac incorporated in nano-emulsions, nano-emulgels, and a colloidal suspension. *Drug Deliv Transl Res*. 2023;13(5):1372–89. <https://doi.org/10.1007/s13346-022-01267-7>.
 39. Herman A, Herman AP. Essential oils and their constituents as skin penetration enhancer for transdermal drug delivery: a review. *J Pharm Pharmacol*. 2015;67(4):473–85. <https://doi.org/10.1111/jphp.12334>.
 40. Van Zyl L, Du Preez J, Gerber M, Du Plessis J, Viljoen J. Essential fatty acids as transdermal penetration enhancers. *J Pharm Sci*. 2016;105(1):188–93. <https://doi.org/10.1016/j.xphs.2015.11.032>.
 41. Fox LAM. Ivermectin: uses and impact 20 years on. *Curr Opin Infect Dis*. 2006;19(6):588–93. <https://doi.org/10.1097/QCO.0b013e328010774c>.
 42. Awad H, Rawas-Qalaji M, El Hosary R, Jagal J, Ahmed IS. Formulation and optimization of ivermectin nanocrystals for enhanced topical delivery. *Int J of Pharm: X*. 2023;6: 100210. <https://doi.org/10.1016/j.ijpx.2023.100210>.
 43. Das S, Lee SH, Chia VD, Chow PS, Macbeath C, Liu Y, Shlieout G. Development of microemulsion based topical ivermectin formulations: pre-formulation and formulation studies. *Colloids Surf B*. 2020;189: 110823. <https://doi.org/10.1016/j.colsurfb.2020.110823>.
 44. Starkloff WJ, Bucalá V, Palma SD, Gonzalez Vidal NL. Design and in vitro characterization of ivermectin nanocrystals liquid formulation based on a top-down approach. *Pharm Dev Technol*. 2017;22(6):809–17. <https://doi.org/10.1080/10837450.2016.1200078>.
 45. Blagden N, de Matas M, Gavan PT, York P. Crystal engineering of active pharmaceutical ingredients to improve solubility and dissolution rates. *Adv Drug Deliv Rev*. 2007;59(7):617–30. <https://doi.org/10.1016/j.addr.2007.05.011>.

46. Good DJ, Nafr RH. Solubility advantage of pharmaceutical cocrystals. *Cryst Growth Des.* 2009;9(5):2252–64. <https://doi.org/10.1021/cg801039j>.
47. Macrae CF, Sovago I, Cottrell SJ, Galek PT, McCabe P, Pidcock E, et al. Mercury 4.0: From visualization to analysis, design and prediction. *J Appl Crystallogr.* 2020;53(1):226–35. <https://doi.org/10.1107/S1600576719014092>.
48. Schrödinger LLC. The PyMOL Molecular Graphics System, Version 1.8. 2015.
49. Eberhardt J, Santos-Martins D, Tillack AF, Forli S. AutoDock Vina 1.2. 0: New docking methods, expanded force field, and python bindings. *J Chem Inf Model.* 2021;61(8):3891–8. <https://doi.org/10.1021/acs.jcim.1c00203>.
50. Drake FL, Rossum GV. Python 3 reference manual. Python Software Foundation. 2009;2(3).
51. Seabold S, Perktold J. Econometric and statistical modeling with python. In: Van der Walt SJ, editor. *Proceedings of the 9th Python in Science Conference*. Austin, TX: Python for Scientific Computing. 2010;28. pp. 92–6.
52. McKinney W. Data structures for statistical computing in Python. In: Van der Walt SJ, editor. *Proceedings of the 9th Python in Science Conference*. Austin, TX: Python for Scientific Computing. 2010;445. pp. 51–6.
53. Harris CR, Millman KJ, van der Walt SJ, Gommers R, Virtanen P, Cournapeau D, et al. Array programming with NumPy. *Nature.* 2020;585(7825):357–62. <https://doi.org/10.1038/s41586-020-2649-2>.
54. Hunter JD. Matplotlib: a 2D graphics environment. *Comput Sci Eng.* 2007;9(3):90–5. <https://doi.org/10.1109/MCSE.2007.55>.
55. Waskom M. Seaborn: statistical data visualization. *J Open Source Softw.* 2021;6(60):3021.
56. Shubin K, Bērziņš A, Belyakov S. Crystal structures of new ivermectin pseudopolymorphs. *Crystals.* 2021;11(2):172. <https://doi.org/10.3390/cryst11020172>.
57. Damera DP, Nag A. Tuning the phase transition temperature of hybrid Span60-L64 thermoresponsive niosomes: Insights from fluorescence and Raman spectroscopy. *J Mol Liq.* 2021;340:117110. <https://doi.org/10.1016/j.molliq.2021.117110>.
58. Orendorff CJ, Ducey MW, Pemberton JE. Quantitative correlation of Raman spectral indicators in determining conformational order in alkyl chains. *J Phys Chem A.* 2002;106(30):6991–8. <https://doi.org/10.1021/jp014311n>.
59. Mandalaywala R, Rana A, Ramos AL, Sampson P, Ashkenas J. Physical and pharmacokinetic characterization of Soluvec™, a novel, solvent-free aqueous ivermectin formulation. *Ther Deliv.* 2023;14(6):391–9. <https://doi.org/10.4155/tde-2023-0021>.

Publisher's Note Springer Nature remains neutral with regard to jurisdictional claims in published maps and institutional affiliations.